Spectroscopic, Thermal, and Magnetic Properties of Metal/TCNQ Network Polymers with Extensive Supramolecular Interactions between Layers

H. Zhao, R. A. Heintz, X. Ouyang, and K. R. Dunbar*,†

Contribution from the Department of Chemistry and The Center for Fundamental Materials Research, Michigan State University, East Lansing, Michigan 48824

C. F. Campana

Bruker AXS, INC. Analytical X-ray Systems, 6300 Enterprise Lane, Madison, Wisconsin 53719-1173

R. D. Rogers

Department of Chemistry, The University of Alabama, Tuscaloosa, Alabama 35487

Received August 31, 1998. Revised Manuscript Received December 14, 1998

Reactions of $[M(MeCN)_n][BF_4]_2$ salts with $Bu_4N(TCNQ)$ in MeOH yield $M(TCNQ)_2(MeOH)_x$ (M = Mn, **1**; Fe, **2**; Co, **3**; Ni, **4**, $x = 2-4$), and reactions of $MnCl_2$, $FeSO_4 \cdot 7H_2O$, $CoSO_4 \cdot 7H_2O$ and $NiCl_2 \cdot 6H_2O$ in H_2O produce $M(TCNQ)_2(H_2O)_2$ (M = Mn, **5**; Fe, **6**; Co, **7**; Ni, **8**). Infrared spectroscopy, powder X-ray diffraction and thermogravimetric analyses of **1**−**8** indicate that the products prepared in the same solvent constitute isostructural families of compounds. $[Mn(TCNQ-TCNQ)(MeOH)_4]_\infty$ (**9**) crystallizes in the triclinic space group $P\bar{1}$, $a = 7.2966(8)$ Å, $b = 7.4289(8)$ Å, $c = 14.060(2)$ Å, $\alpha = 76.112(2)°$ $\beta = 87.242(2)°$, $\gamma = 71.891(2)°$, $V = 702.91(13)$ Å^3, $Z = 1$; $[Mn(TCNQ)(TCNQ-TCNQ)_{0.5}(MeOH)_2]_\infty$ (**10**) crystallizes in the monoclinic space group $C2/c$, $a = 14.4378(5)$ Å, $b = 27.3067(11)$ Å, $c = 13.1238(5)$ Å, $\beta = 90.057(1)°$, $V = 5174.0(3)$ Å^3, $Z = 8$. Compound **9** contains $TCNQ^-$ ligands that have undergone an unusual σ-dimerization to $[TCNQ-TCNQ]^{2-}$ that acts as a tetradentate ligand to Mn(II) ions to give a 2-D staircase polymeric motif. The layers are connected by hydrogen-bonds between axially coordinated MeOH from adjacent layers and MeOH located between the layers. Compound **10** exhibits a zigzag polymeric motif with equatorially bound TCNQ-derived ligands of two types; the edges of the layers consist of cis-μ-$TCNQ^-$ molecules involved in π-stacking with $TCNQ^-$ units from another layer and σ-$[TCNQ-TCNQ]^{2-}$ acting as a tetradentate bridging ligand. Axial MeOH ligands are hydrogen-bonded to dangling nitrile groups of *cis*-μ-$TCNQ^-$ ligands in the next layer. $Mn(TCNQ)_2(H_2O)_2$ (**11**) crystallizes in the monoclinic space group $I2/a$, $a = 12.5843(7)$ Å, $b = 13.7147(7)$ Å, $c = 13.3525(70$ Å, $\beta = 92.887(1)°$, $V = 2301.58$ Å^3, $Z = 4$. This material adopts a double-layer motif consisting of Mn(II) ions bonded to *syn*-μ_2-$TCNQ^-$ equatorial ligands and axial H_2O molecules. Compounds **1**−**11** exhibit Curie−Weiss behavior with weak antiferromagnetic coupling being observed at low temperatures. The Zn(II) analogue of **10**, $[Zn(TCNQ)(TCNQ-TCNQ)_{0.5}(MeOH)_2]_\infty$ (**12**) was also prepared: space group $C2/c$, $a = 14.2252(1)$ Å, $b = 27.3290(4)$ Å, $c = 13.1177(2)$ Å, $\beta = 90.074(1)°$, $V = 5099.64(11)$ Å^3, $Z = 8$. Powder X-ray diffraction was used to probe structures **1**−**11**, and it was found that **9** converts to a new phase with heating or exposure to X-rays that is related to disruption of the σ-dimer $(TCNQ-TCNQ)^{2-}$ ligands and loss of MeOH. The new phase, whose powder pattern is identical with that of a phase prepared from MeCN, exhibits ferromagnetic behavior.

Introduction

Charge-transfer materials based on organic donors and acceptors have been under investigation for nearly four decades, beginning with the first reports of conducting salts of organocyanide acceptors such as TCNQ.[1] One of the main issues in low-dimensional salts composed of planar organic radicals is the mode of stacking. The solid-state arrangement of the ions has a dramatic effect on the resulting magnetic and charge-transport properties; for example charge-transfer salts such as [TTF][TCNQ] that crystallize with segregated stacks of donors and acceptors typically exhibit high electrical conductivity whereas those that assemble in integrated stacks of alternating donors and acceptors tend to show interesting optical as well as magnetic properties.[2]

In light of the promise for the use of tunable organic donor and acceptor molecules in materials applications,

* To whom correspondence should be addressed.
† E-mail: dunbar@cem.msu.edu.

10.1021/cm980608v CCC: $18.00
Published on Web 02/17/1999

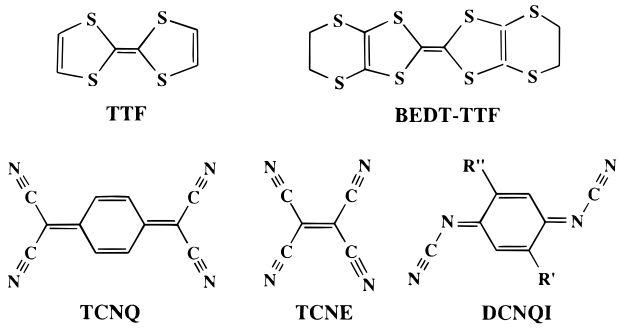

Figure 1. Schematic diagrams of organic donors and acceptors used in charge-transfer materials.

researchers are incorporating molecules of the types depicted in Figure 1 into complex solids with multidimensional frameworks that involve a paramagnetic inorganic component.[3] Interest in hybrid organic/inorganic materials has been heightened by the recent reports of (BEDT−TTF) salts of paramagnetic metal anions that are highly conducting and even superconducting.[4]

One synthetic strategy to materials that contain both metals and organic acceptors is the combination of metal cations with organic acceptor anions such as $TCNQ^{-\bullet}$ (7,7,8,8-tetracyanoquinodimethane),[5] $TCNE^{-\bullet}$ (tetracyanoethylene)[6] and $DCNQI^{-\bullet}$ (*N*,*N*′-dicyanoquinonediimine).[7] In this manner one can take advantage of the tendency for planar organic radicals to engage in π-stacking interactions, while at the same time imparting new properties based on the presence of metal-based electrons. Among the interesting materials that have emerged from these studies are metallic polymers of Cu with DCNQI,[7] electrically bistable materials of Cu and Ag with TCNQ,[8] and a room-temperature bulk ferromagnet of V with TCNE.[6a] Notably, all of these materials are binary compounds composed only of metals and organic acceptors with no co-ligands to reduce the dimensionality of the extended arrays. Unfortunately, polymeric materials of this type are notoriously difficult to crystallize, a fact that has hampered research efforts aimed at magnetostructural correlations. We have found, however, that with the proper selection of starting materials and solvents it is possible to prepare crystalline, neutral framework compounds with metal ions bridged only by ligands derived from $TCNQ^{-}$.

In this paper we report the syntheses and characterization of products from reactions involving Mn(II), Fe(II), Co(II), Ni(II), and Zn(II) ions with and $TCNQ^{-}$. Representative single-crystal X-ray structures, powder X-ray data, infrared spectral properties and magnetic properties are discussed in light of the TCNQ packing motif that is adopted in the solid-state. Also detailed is the solid-state conversion of $Mn(TCNQ)_2(MeOH)_2$ from a paramagnetic crystalline phase to an ordered phase that displays ferromagnetic behavior. A portion of this work was previously published in communication form.[5j]

(1) (a) Acker, D. S.; Harder, R. J.; Hertler, W. R.; Mahler, W.; Melby, L. R.; Bensin, R. E.; Mochel, W. E. *J. Am. Chem. Soc.* **1960**, *82*, 6408. (b) Melby, L. R.; Harder, R. J.; Hertler, W. R.; Mahler, W.; Benson, R. E.; Mochel, W. E. *J. Am. Chem. Soc.* **1962**, *84*, 3374. (c) Torrance, J. B. *Acc. Chem. Res.* **1979**, *12*, 79. (d) Endres H. In *Extended Linear Chain Compounds*; Miller, J. S. Ed.; Plenum: New York. **1983**; Vol. 3, pp 263−312. (e) Wudl, F. *Acc. Chem. Res.*, **1984**, 17, 227. (f) Jérome, D. *Science* **1991**, *252*, 1509. (e) Bryce, M. R. *Chem. Soc. Rev.* **1991**, *20*, 355. (g) Williams, J. M.; Schultz, A. J.; Geiser, U.; Carlson, K. D.; Kini, A. M.; Wang, H. H.; Kwok, W.-K.; Whangbo, M.-H.; Schirber, J. E. *Science* **1991**, *252*, 1501. (h) Ward, M. D. *Electroanal Chem.* **1988** *16*, 181. (i) Martin, N.; Segura, J. L.; Seoane, C. *J. Mater. Chem.* **1997**, *7*, 1661.

(2) (a) Miller, J. S.; Calabrese, J. C.; Epstein, A. J.; Bigelow, R. W.; Zhang, J. H.; Reiff, W. M. *J. Chem. Soc., Chem. Commun.* **1986**, 1026. (b) Miller, J. S.; Zhang, J. H.; Reiff, W. M.; Dixon, D. A.; Preston, L. D.; Reis, A. H.; Gebert, E.; Extine, M.; Troup, J.; Epstein, A. J.; Ward, M. D. *J. Phys. Chem.* **1987**, *91*, 4344. (c) Broderick, W. E.; Thompson, J. A.; Day, E. P.; Hoffman, B. M. *Science* **1990**, *249*, 401. (d) Kollmar, C.; Couty, M.; Kahn, O. *J. Am. Chem. Soc.* **1991**, *113*, 7994. (d) Miller, J. S.; Epstein, A. J. *Angew. Chem., Int. Ed. Engl.* **1994**, *33*, 385. (e) Murphy, V. J.; O'Hare, D. *Inorg. Chem.* **1994**, *33*, 1833.

(3) (a) Pénicaud, A.; Batail, P.; Perrin, C.; Coulon, C.; Parkin, S. S. P.; Torrance, J. B. *J. Chem. Soc., Chem. Commun.* **1987**, 330. (b) Davidson, A.; Boubekeur, K.; Pénicaud, A.; Auban, P.; Lenoir, C.; Batail, P.; Hervé, G. *J. Chem. Soc. Chem. Commun.* **1989**, 1373−1374. (c) Pénicaud, A.; Boubekeur, K.; Batail, P.; Canadell, E.; Auban-Senzier, P.; Jérome *J. Am. Chem. Soc.* **1993**, *115*, 4101−4112. (d) Coulon, C.; Livage, C.; Gonzalvez, L.; Boubekeur, K.; Batail, P. *J. Phys. I Fr.* **1993**, *3*, 1. (e) Coronado, E.; Gómez-Garcia, C. J. *Comments Inorg. Chem.* **1995**, *17*, 255. (f) Gómez-Garcia, C. J.; Giménez-Saiz, Triki, S.; Coronado, E.; Magueres, P. L.; Ouahab, L.; Ducasse, L.; Sourisseau, C.; Delhaes, P. *Inorg, Chem.* **1995**, *34*, 4139. (g) Coronado, E.; Delhaes, P.; Galáan-Mascarós, J. R.; Giménez-Saiz, C. J. *Synth. Met.* **1997**, *85*, 1647.

(4) (a) Bousseau, M.; Valade, L.; Legros, J.-P.; Cassoux, P.; Garbauskas, M.; Interrante, L. V. *J. Am. Chem. Soc.* **1986**, *108*, 1908. (b) Day, P.; Kurmoo, M.; Mallah, T.; Marsden, I. R.; Allan, M. R.; Friend, R. H.; Pratt, F. L.; Hayes, W.; Chasseau, D.; Bravic, G.; Ducasse, L. *J. Am. Chem. Soc.* **1992**, *114*, 10722. (c) Kurmoo, M.; Graham, A. W.; Day, P.; Coles, S. J.; Hursthouse, M. B.; Caulfield, J. L.; SIngleton, J.; Pratt, F. L.; Hayes, W.; Ducasse, L.; Guionneau, P. *J. Am. Chem. Soc.* **1995**, *117*, 12209; see also references therein.

(5) (a) Lacroix, P.; Kahn, O.; Gliezes, A.; Valade, L.; Cassoux, P. *Nouv. J. Chim.* **1985**, 643−651. (b) Bartley, S. L.; Dunbar, K. R. *Angew. Chem., Int. Ed. Eng.* **1991**, *30*, 448. (c) Ballester, L.; Barral, M.; Gutiérrez, A.; Jiménez-Aparicio, R.; Martinez-Muyo, J.; Perpiñan, M.; Monge, M.; Ruiz-Valero, C. *J. Chem. Soc. Chem. Commun.* **1991**, 1396−1397. (c) Cornelissen, J. P.; van Diemen, J. H.; Groeneveld, L. R.; Haasnoot, J. G.; Spek, A. L.; Reedijk, J. *Inorg. Chem.* **1992**, *31*, 198−202. (d) Oshio, H.; Ino, E.; Mogi, I,; Ito, T. *Inorg. Chem.* **1993**, *32*, 5697−5703. (e) Dunbar, K. R.; Ouyang, X. *Mol. Cryst. Liq. Cryst.* **1995**, *273*, 21−28. (f) Kaim, W.; Moscherosch, M. *Coord. Chem. Rev.* **1994,** *129*, 157. (g) Dunbar, K. R. *Angew Chem., Int. Ed. Engl.* **1996**, *35*, 1659. (h) Decurtins, S.; Dunbar, K. R.; Gomez-Garcia, C. J.; Mallah, T.; Raptis, R. G.; Talham, D.; Veciana, J. In *Molecular Magnetism: From Molecular Assemblies to the Devices*; Coronado, E., Delhaès, P., Gatteschi, D., Miller, J. S., Eds.; NATO ASI Series E321; Kluwer: Dordrecht, The Netherlands, 1996; pp 571−582. (i) Dunbar, K. R.; Ouyang, X. *Chem. Commun.*, **1996**, 2427. (j) Zhao, H.; Heintz, R. A.; Rogers, R. D.; Dunbar, K. R. *J. Am. Chem. Soc.* **1996**, *118*, 12844. (k) Dunbar, K. R.; Ouyang, X. *Inorg. Chem.* **1996**, *35*, 7188. (l) Azcondo, M. T.; Ballester, L.; Gutiérrez, A.; Perpiñán, F.; Amador, U.; Ruiz-Valero, C.; Bellitto, C. *J. Chem. Soc., Dalton Trans.* **1996**, 3015.

(6) (a) Manriquez, J. M.; Yee, G. T.; McLean, R. S.; Epstein, A. J.; Miller, J. S. *Science* **1991**, *252*, 1415. (b) Miller, J. S.; Calabrese, J. C.; McLean, R. S.; Epstein, A. J. *Adv. Mater.* **1992**, *4*, 498. (c) Miller, J. S.; Vazquez, C.; Jones, N. L.; McLean, R. S.; Epstein, A. J. *J. Mater. Chem.* **1995**, *5*, 707. (d) Miller, J. S.; Calabrese, J. C.; Vazquez, C.; Calabrese, J. C.; McLean, R. S.; Epstein, A. J. *Adv. Mater.* **1994**, *6*, 217. (e) Böhm, A.; Vazquez, C.; McLean, R. S.; Calabrese, J. C.; Kalm, S. E.; Manson, J. L.; Epstein, A. J.; Miller, J. S. *Inorg. Chem.* **1996**, *35*, 3083. (f) Brinckerhoff, W. B.; Morin, B. G.; Brandon, E. J.; Miller, J. S.; Epstein, A. J. *J. Appl. Phys.* **1996**, *79*, 6147.

(7) (a) Aumüller, A.; Erk, P.; Klebe, G.; Hünig, S.; von Schütz, J.; Werner, H. *Angew. Chem., Int. Ed. Engl.* **1986**, *25*, 740−741. (b) Aumüller, A.; Erk, P.; Hünig, S. *Mol. Cryst. Liq. Cryst. Inc. Nonlin. Opt.* **1988**, *156*, 215−221. (c) Erk, P.; Gross, H.-J.; Hünig, U. L.; Meixner, H.; Werner, H.-P.; von Schütz, J. U.; Wolf, H. C. *Angew. Chem., Int. Ed. Engl.* **1989**, *28*, 1245−1246. (d) Kato, R.; Kobayashi, H.; Kobayashi, A. *J. Am. Chem. Soc.* **1989**, *111*, 5224−5232. (e) Aumüller, A.; Erk, P.; Hünig, S.; Hädicke, E.; Peters, K.; von Schnering, H. G. *Chem Ber.* **1991**, *124*, 2001. (f) Sinzger, K.; Hünig, S.; Jopp, M.; Bauer, D.; Bietsch, W.; von Schütz, J. U.; Wolf, H. C.; Kremer, R. K.; Metzenthin, T.; Bau, R.; Khan, S. I.; Lindbaum, A.; Lengauer, C. L.; Tillmanns, E. *J. Am. Chem. Soc.* **1993**, *115*, 7696.

(8) (a) Potember, R. S.; Poehler, T. O.; Cowan, D. O. *Appl. Phys. Lett.* **1979**, *34*, 405 (b) Potember, R. S.; Poehler, T. O.; Cowan, D. O.; Carter, F. L.; Brant, P. In *Molecular Electronic Devices II*; Carter, F. L., Ed.; Marcel Dekker: New York, 1982; p 91. (c) Hoagland, J. J.; Wang, X. D.; Hipps, K. W. *Chem. Mater.* **1993**, *5*, 54. (d) Dunbar, K. R.; Cowen, J.; Heintz, R. A.; Grandinetti, G.; Ouyang, X.; Zhao, H. *Inorg. Chem.* **1999**, *38*, 144.

Table 1. Crystallographic Data for $[Mn(TCNQ-TCNQ)(MeOH)_4]_\infty$ (9), $[Mn(TCNQ)(TCNQ-TCNQ)_{0.5}(MeOH)_2]_\infty$ (10), $[Mn(TCNQ)_2(H_2O)_2]_\infty$ (11), and $[Zn(TCNQ)(TCNQ-TCNQ)_{0.5}(MeOH)_2]_\infty$ (12)

compound	9	10	11	12
formula	$MnN_8O_4C_{28}H_{24}$	$MnN_8O_2C_{26}H_{16}$	$MnN_8O_2C_{24}H_{12}$	$ZnN_8O_2C_{26}H_{16}$
fw	591.49	527.41	499.36	537.84
temp (°C)	-150 ± 1	-100 ± 1	-100 ± 1	-100 ± 1
space group	$P\bar{1}$	*C*2/*c*	*I*2/*a*	*C*2/*c*
a, Å	7.2966(8)	14.4378(5)	12.5843(7)	14.2252(1)
b, Å	7.4289(8)	27.3067(1)	13.7147(7)	27.3290(4)
c, Å	14.060(2)	13.1238(5)	13.3525(7)	13.1177(2)
α, deg	76.112(2)	90	90	90
β, deg	87.242(2)	90.057(1)	92.8870(10)	90.074(1)
γ, deg	71.891(2)	90	90	90
V, Å^3	702.91(13)	5174.0(3)	2301.6(2)	5099.64(11)
Z	1	8	4	8
d_{calc}(g/cm^3)	1.397	1.354	1.441	1.401
μ (mm^{-1})	0.518	0.549	0.613	1.003
radiation	Mo Kα graphite monochromated $\lambda_\alpha = 0.710\ 73$ Å			
total no. of data	2870	10394	6950	15633
no. of unique data	1967	3724	2681	5949
R1[a]	0.0687	0.0678	0.0357	0.0386
wR2[b]	0.1546	0.1210	0.0794	0.0842
GooF[c]	1.321	1.216	1.077	1.066

[a] $R1 = \sum ||F_o| - |F_c||/\sum |F_o|$. [b] $wR2 = [\sum[w(F_o^2 - F_c^2)^2]/\sum[w(F_o^2)^2]]^{1/2}$. [c] $GooF = S = [\sum[w(F_o^2 - F_c^2)^2]/(n - p)]^{1/2}$.

Experimental Section

Starting Materials and Reaction Procedures. All reactions were carried out under an argon atmosphere by the use of standard Schlenk-line techniques. $MnCl_2$, $FeSO_4 \cdot H_2O$, $CoSO_4 \cdot 7H_2O$, and $NiCl_2 \cdot 6H_2O$ were obtained from commercial sources and used without further purification. $[M(MeCN)_{4,6}][BF_4]_2$ precursors were prepared as described in the literature.[9] LiTCNQ was prepared by combining TCNQ and 3 equivalents of LiI in hot acetonitrile and allowing the mixture to cool for 12 h. Bu_4N(TCNQ) was prepared by metathesis of LiTCNQ with Bu_4NI in boiling water followed by recrystallization from CH_2Cl_2.[1a,b] Acetonitrile and methanol were predried over 4 Å molecular sieves and freshly distilled under a nitrogen atmosphere from CaH_2 and $Mg(OCH_3)_2$, respectively.

Syntheses of $M(TCNQ)_2(MeOH)_x$ (M = Mn (1), Fe (2), Co (3), and Ni (4)). A MeOH solution (20 mL) of (Bu_4N)TCNQ (0.447 g, 1.00 mmol) was slowly added to a MeOH solution (10 mL) of $[Mn(MeCN)_4][BF_4]_2$ (0.197 g, 0.5 mmol), $[Fe(MeCN)_6][BF_4]_2$ (0.238 g, 0.50 mmol), $[Co(MeCN)_6][BF_4]_2$ (0.240 g, 0.5 mmol), or $[Ni(MeCN)_6][BF_4]_2$ (0.240 g, 0.50 mmol). The resulting reaction solution was stirred for 20 min to give a blue precipitate that was collected by filtration, washed with methanol followed by diethyl ether, and dried in vacuo. Yields: (**1**) 0.187 g, 71%; (**2**) 0.184 g, 70%; (**3**) 0.180 g, 69%; (**4**) 0.175 g, 66%. The number of solvent molecules *x* varies between 2 and 4, and depends on the amount of time that the sample is subjected to a vacuum and the identity of the metal. Anal. Mn ($x = 2$) Calcd for $C_{26}H_{16}MnN_8O_2$: C, 59.21; H, 3.06; N, 21.25. Found: C, 59.53; H, 2.41; N, 21.71. Fe ($x = 2$) Calcd for $C_{26}H_{16}FeN_8O_2$: C, 59.11; H, 3.05; N, 21.21 Found: C, 58.65; H, 3.17; N, 19.95. Co ($x = 3$) Calcd for $C_{27}H_{20}CoN_8O_3$: C, 57.56; H,3.58; N, 19.89. Found: C, 57.32; H, 2.75; N, 19.92. Ni ($x = 4$) Calcd for $C_{28}H_{24}NiN_8O_4$: C, 56.50; H, 4.06; N, 18.83. Found: C, 55.47; H, 2.91; N, 19.13. Thermogravimetric measurements indicate that the samples are stable with approximately 2 equiv of coordinated MeOH.

Syntheses of $M(TCNQ)_2(H_2O)_2$ (M = Mn (5), Fe (6), Co (7), and Ni (8)). An aqueous solution (20 mL) of LiTCNQ (0.211 g, 1.0 mmol) was added to an aqueous solution (20 mL) of $MnCl_2$ (0.063 g, 0.5 mmol), $FeSO_4 \cdot 7H_2O$(0.139 g, 0.5 mmol), $CoSO_4 \cdot 7H_2O$(146 g, 0.5 mmol) or $NiCl_2 \cdot 6H_2O$(0.119 g, 0.5 mmol) with stirring at room temperature. The resulting blue precipitate was collected by filtration after 20 min, washed with water followed by ethanol and diethyl ether, and finally dried in vacuo. Yields: 0.242 g, 94% for Mn(II); 0.222 g, 86% for Fe(II); 0.243 g, 93% for Co(II); 0.233 g, 89% for Ni(II). Anal. Calcd for $C_{24}H_{12}MnN_8O_2$: C, 57.73; H, 2.40; N, 22.44. Found: C, 57.76; H, 2.20; N,22.47. Calcd for $C_{24}H_{12}FeN_8O_2$: C, 57.62; H, 2.41; N, 22.40. Found: C 57.26; H, 2.33; N, 22.02. Calcd for $C_{24}H_{12}CoN_8O_2$: C, 57.27; H, 2.40; N, 22.26. Found: C, 57.41; H, 2.10; N, 22.26. Calcd for $C_{24}H_{12}NiN_8O_2$: C, 57.30; H, 2.40; N, 22.27. Found: C, 57.17; H, 2.16; N, 22.05.

Single-Crystal Growth. Blue parallelepiped crystals of $[Mn(TCNQ-TCNQ)(MeOH)_4]_\infty$ (**9**) were grown by slow diffusion of methanolic solutions of $[Mn(MeCN)_4][BF_4]_2$ and Bu_4N(TCNQ). Purple needles of $[Mn(TCNQ)(TCNQ-TCNQ)_{0.5}(MeOH)_2]_\infty$ (**10**) were grown by slow diffusion of a methanolic solution of $[Mn(MeCN)_4][BF_4]_2$ into a mixture of MeCN/MeOH (2:1) containing Bu_4N(TCNQ). Red-purple monoclinic prisms of $[Mn(TCNQ)_2(H_2O)_2]_\infty$ (**11**) were grown by slow diffusion of aqueous solutions of $MnBr_2$ and LiTCNQ. Slow diffusion of methanolic solution of $[Zn(MeCN)_4][BF_4]_2$ and LiTCNQ in a MeCN/MeOH mixture led to purple needles of $[Zn(TCNQ)(TCNQ-TCNQ)_{0.5}(MeOH)_2]_\infty$ (**12**). The crystals of **10**, **11**, and **12** were grown in 3 mm diameter sealed Pyrex tubes.

Physical Measurements. Infrared spectra were recorded as Nujol mulls in the range 400−4800 cm^{-1} on a Nicolet IR/42 spectrophotometer. Powder X-ray diffraction data were collected on a Rigaku RU200B powder diffractometer with CuKα radiation in the range 5−50° in steps of 0.02° in 2*θ*. Thermogravimetric analyses were performed between 25 and 1000 °C on a SHIMADZU, TGA-50. Magnetic susceptibility data were collected on a Quantum Design, Model MPMS, superconduting quantum interference device between 5 and 320 K at fields of 500 or 1000 G.

X-ray Crystallographic Procedures. Crystals of **9** (0.05 × 0.10 × 0.10 mm), **10** (0.10 × 0.10 × 0.40 mm), **11** (0.20 × 0.20 × 0.20 mm), and **12** (0.20 × 0.20 × 0.60 mm) were mounted on glass fibers and secured with grease. Diffraction data were collected on Siemens SMART CCD area detector instruments at −150 (1) °C for **9** and −100 (1)°C for **10**, **11**, and **12**. A summary of data collection parameters for compounds **9**−**12** is given in Table 1. The data were solved and refined in SHELXTL V. 5.0 by full-matrix least-squares on F^2. The original cell and systematic absences for **10** suggested an orthorhombic *C*-centered crystal system, but the structure was ultimately solved as a 50/50 twin in *C*2/*c* (twinning law 100, 010, 00$\bar{1}$). The disordered MeOH group was modeled in two orientations with occupancies of 0.45 C(25) and 0.55 C(25′). Refinement of a batch scale factor revealed that the twinning was 70/30 in the crystal of **12** compared to 50/50 in the structure of **10**. All non-hydrogen atoms were located and refined with anisotropic thermal parameters, and hydrogen atoms were located from difference Fourier maps and refined

(9) Hathaway, B. J.; Holah, D. G.; Underhill, A. E. *J. Chem. Soc.* **1962**, 2444.

Table 2. Selected Bond Distances (Å) and Angles (deg) for Compounds 9−12

[Mn(TCNQ−TCNQ)(MeOH)$_4$]$_\infty$ (**9**)			
Mn−O1	2.172(4)	Mn−N1	2.219(4)
N1−C8	1.148(6)	C1−C7	1.464(7)
C7−C9	1.402(7)	C10−C10′	1.659(10)
O1−Mn−O′	180.0	C4−C10−C11	112.0(4)
C4−C10−C12	111.4(4)	C4−C10−C10A	111.8(5)
C6−C1−C7	119.8(4)	N3−C11−C10	177.7(6)
[Mn(TCNQ)(TCNQ−TCNQ)$_{0.5}$(MeOH)$_2$]$_\infty$ (**10**)			
Mn1−N1	2.226(6)	Mn1−N5	2.183(6)
Mn1−O1	2.191(5)	Mn2−O2	2.161(5)
Mn2−N6	2.161(6)	N1−C8	1.129(8)
N5−C20	1.151(8)	C1−C7	1.421(7)
C1−C3	1.364(9)	C4−C10	1.404(8)
C11−N3	1.147(9)	C13−C19	1.459
C14−C15	1.393(9)	C22−C22′	1.635 (10)
N1−Mn1−N5	87.9(2)	O1−Mn1−O1′	175.1(3)
C16−C22−C22′	112.6(5)	C4−C10−C11	122.3(6)
[Mn(TCNQ)$_2$(H$_2$O)$_2$]$_\infty$ (**11**)			
Mn1−N1	2.225(2)	Mn1−O1	2.142(2)
N1−C8	1.147(2)	N2−C9	1.149(2)
C1−C7	1.419(2)	C2−C3	1.363(2)
C4−C10	1.419(2)	C9−N2′	1.149(2)
C11−N3	1.151(2)	C12−N4	1.147(2)
O1−Mn1−O1′	180	O1−Mn1−N1′	90.62(6)
N1−Mn1−N1′	180	O1A−Mn1A−N4′	91.92(6)
Mn1−N1−C8	161.5(2)		
[Zn(TCNQ)(TCNQ−TCNQ)$_{0.5}$(MeOH)$_2$]$_\infty$ (**12**)			
Zn1−N1	2.154(3)	Zn1−N5	2.092(3)
Zn1−O1	2.112(3)	Zn2−O2	2.098(3)
Zn2−N2	2.165(3)	Zn2−N6	2.084(2)
N1−C8	1.151(4)	N5−C20	1.149(4)
C1−C7	1.431(4)	C2−C3	1.365(4)
C4−C10	1.425(4)	C11−N3	1.160(4)
C13−C19	1.461(3)	C14−C15	1.392(4)
C22−C22′	1.641(5)		
N1−Zn1−N5	88.21(11)	O1−Zn1−O1′	172.87(14)
O2−Zn2−N6	92.83(11)	C4−C10−C11	120.6(3)
C16−C22−C22′	112.2(3)		

with isotropic thermal parameters. Final atomic parameters and equivalent isotropic thermal parameters for non-hydrogen atoms are deposited in the Supporting Information. Important distances and angles in **9**−**12** are listed in Table 2.

Results and Discussion

Syntheses. Reactions of the acetonitrile starting materials [M(MeCN)$_x$][BF$_4$]$_2$ (M = Mn, x = 4; Fe, Co, Ni, Zn, x = 6)[9] with (Bu$_4$N)TCNQ in MeOH and $MnCl_2$, $FeSO_4 \cdot 7H_2O$, and $CoSO_4 \cdot 7H_2O$ $NiCl_2 \cdot 6H_2O$ with LiTCNQ in H_2O lead to the rapid formation of dark blue-purple crystalline solids. These materials are robust under ambient conditions of exposure to air, moisture, and light, with no decomposition being detected after several months. Elemental analyses for the water compounds fit the empirical formula M(TCNQ)$_2$(H$_2$O)$_2$ rather than M(TCNQ)$_2$(H$_2$O)$_3$ which had been previously reported.[10a−e] Presumably, handling and storage conditions affect the quantity of water that these materials retain, which is an important point because degree of hydration is known to influence the magnetic properties of these aqueous-derived materials.[10b]

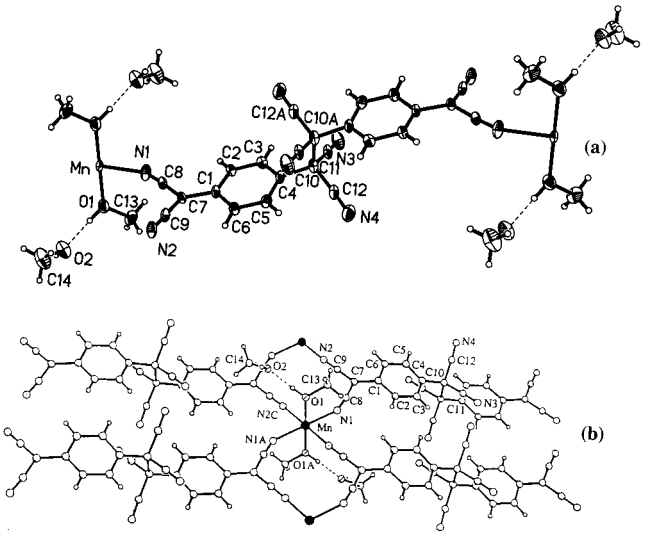

Figure 2. (a) ORTEP plot of the asymmetric unit in [Mn(TCNQ−TCNQ)(MeOH)$_4$]$_\infty$ (**9**) with atoms depicted as 50% probability ellipsoids and (b) Pluto diagram showing immediate coordination sphere with hydrogen bonding.

No prior reports of binary metal/TCNQ compounds prepared in alcohols have appeared in the literature to our knowledge. Analytical data for the methanol products support the formulations M(TCNQ)$_2$(MeOH)$_x$ ($x \approx 2$, Mn, Fe; $x \approx 3$, Co; $x \approx 4$, Ni). Freshly prepared samples contain more methanol (between 3 and 4 molecules), whereas samples that have been subjected to a prolonged vacuum retain two of the solvent molecules according to TGA.

Description of the Structures. [Mn(TCNQ−TCNQ)(MeOH)$_4$]$_\infty$ (**9**). Crystals of **9** are composed of a 2-D network of six-coordinate Mn(II) ions equatorially bound to the four outer nitrile groups of μ_4-[TCNQ−TCNQ]$^{2-}$ which is a ligand derived from sigma dimerization of two TCNQ$^-$ molecules. An ORTEP diagram of the asymmetric unit and the immediate coordination sphere of **9** are provided in Figure 2, and extended views that emphasize interlayer interactions are depicted in Figure 3. Key bond length and bond angle information is provided in Tables 2 and 3.

The [TCNQ−TCNQ]$^{2-}$ entity has been documented only three previous times, and in these instances it behaves solely as an outer-sphere anion.[11] In the compound [EtP](TCNQ)$_2$ (EtP = *N*-ethylphenazinium),[11a] the σ-[(TCNQ−TCNQ]$^{2-}$ dimer contains a long C−C bond of 1.631(5) Å that joins the two rings, whereas in [Pt(bpy)$_2$][TCNQ−TCNQ][11b] and [Cu(DMP)$_2$]$_2$[TCNQ−TCNQ] (DMP = 2,9-dimethyl-1,10-phenanthroline)[11c] the corresponding distances are 1.65(2) and 1.630(13) Å. A schematic of the σ-dimerized [(TCNQ)$_2$]$^{2-}$ unit in **9** is depicted in Figure 4a. These C−C bonds and the distance found in **9** (1.659 (10) Å or g1−g1′ in Figure 4a) are long, but obviously significant since the C atoms involved are essentially tetrahedral, e.g., C(4)−C(10)-

(10) (a) Melby, L. R.; Harder, R. J.; Hertler, W. R.; Mahler, W.; Benson, R. E.; Mochel, W. E. *J. Am. Chem. Soc.* **1962**, *84*, 3374. (b) Thompson, R. C.; Gujral, V. K.; Wagner, H. J.; Schwerdtfeger, C. F. *Phys. Status Solidi* **1979**, *53*, 181. (c) Chain, E. E.; Kevill, D. N.; Kimball, C. W.; Weber, L. W. *J. Phys. Chem. Solids* **1976**, *37*, 817. (d) Thompson, R. C.; Hoyano, Y.; Schwerdtfeger, C. F. *Solid State Commun.* **1977**, *23*, 633. (e) Kathirgamanathan, P.; Rosseinsky, D. R. *J. Chem. Soc., Chem Commun.* **1980**, 839.

(11) (a) Morosin, B.; Plastas, H. J.; Coleman, L. B.; Stewart J. M. *Acta Crystallogr.* **1978**, *B54*, 540. (b) Dong, V.; Endres, H.; Keller, H. J.; Moroni, W.; Nöthe, D. *Acta Crystallogr., Sect. B* **1977**, *B33*, 2428. (c) Hoffmann, S. K.; Corvan, P. J.; Singh, P.; Sethulekshmi, C. N.; Hatfield, W. E. *J. Am. Chem. Soc.* **1983**, *105*, 4608.

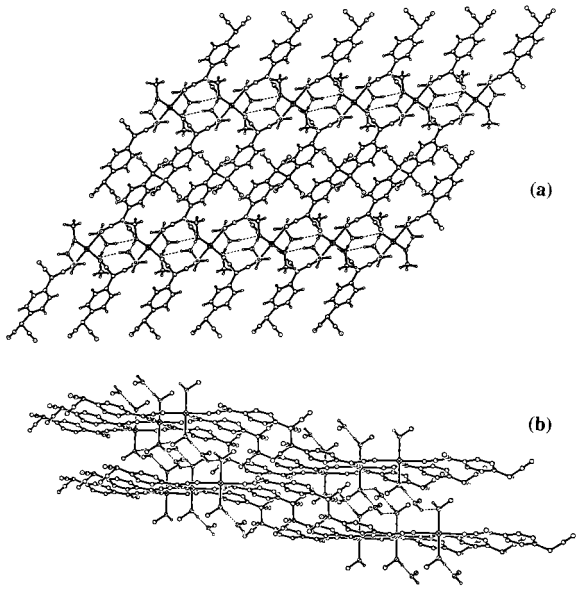

Figure 3. Extended views of **9** (a) top view emphasizing hydrogen-bonding between MeOH molecules and (b) side view of staircase layers.

Table 3. Key Bond Distances (Å) in the TCNQ Unit(s) for 9−12 According to Diagrams in Figure 4

	9	10	11	12
a1−b1	1.402(7)	1.390(10)		1.399(4)
b1−c1	1.464(7)	1.459(7)		1.461(3)
c1−d1	1.397(6)	1.39(1)		1.408(4)
d1−e1	1.376(2)	1.385(8)		1.392(4)
e1−f1	1.394(2)	1.38(2)		1.390(5)
f1−g1	1.524(7)	1.528(7)		1.537(3)
g1−g1′	1.659 (10)	1.635(10)		1.641(5)
g1−h1	1.479(1)	1.48(2)		1.489(5)
a2−b2		1.401(10)		1.421(4)
b2−c2		1.404(8)		1.431(4)
c2−d2		1.43(2)		1.419(4)
d2−e2		1.365(8)		1.365(4)
e2−f2		1.43(1)		1.423(4)
f2−g2		1.421(7)		1.425(4)
g2−h2		1.407(10)		1.416(4)
a3−b3			1.415(2)	
b3−c3			1.419(2)	
c3−d3			1.429(2)	
d3−e3			1.365(2)	
e3−f3			1.430(2)	
f3−g3			1.419(2)	
g3−h3			1.417(2)	

C(10′ = 111.8(5)° in **9**. The uniformity of the distances in the rings (summarized in Table 3), and the significant lengthening of the C═C bond in the planar exocyclic C═C(C≡N)$_2$ groups in the [TCNQ−TCNQ]$^{2-}$ moiety are indications that there is a main contribution from the aromatic resonance structure depicted in Figure 4a. The Mn−N1 distance to the [TCNQ−TCNQ]$^{2-}$ ligand is 2.219(4) Å, which is longer than distances quoted in the literature for 3d metal ions coordinated to TCNQ^{-}.[5,14]

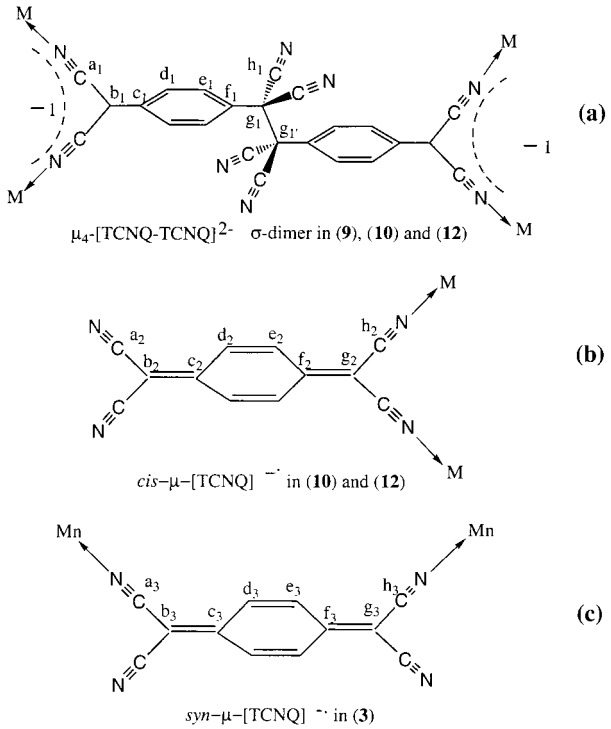

Figure 4. Schematic of the metal binding modes for various forms of TCNQ^{-}: μ_4-[TCNQ−TCNQ]$^{2-}$, *cis*-[μ-TCNQ]$^{-\bullet}$ and *syn*-[μ-TCNQ]$^{-\bullet}$.

For example representative Mn^{II}−N, Fe^{II}−N, and Ni^{II}−N distances, where N is the nitrogen lone pair of a TCNQ^{-} molecule, are 2.153(3),[5d] 2.175(4),[14c] and 2.16(1) Å,[14e] respectively. The tetradentate dianion [TCNQ−TCNQ]$^{2-}$ is nonplanar due to the new sp^3 C−C σ-bond, a situation that leads to a staircase motif for the material; each "step" consists of infinite chains of Mn(II) ions joined by 12-membered metallocyclic rings involving *cis*-nitriles that lie in the same plane. The novel 2-D structure is stabilized in the third dimension by extensive *inter*-layer hydrogen bonding that involves axial MeOH ligands and interstitial MeOH molecules situated between the layers with both linear (O1- -O2 = 2.269 Å; H- - -O2 = 1.738 Å) and bent (O1- -O2A = 2.983 Å; H- - -O2A = 2.277 Å) interactions being present.

[Mn(TCNQ)(TCNQ−TCNQ)$_{0.5}$(MeOH)$_2$]$_\infty$ (10). Crystals of **10** exhibit a 2-D zigzag network of Mn(II) ions coordinated to two different types of TCNQ ligands (Figure 5a). The Mn(II) ions are surrounded by four nitrogen and two oxygen atoms from tetradentate μ_4-[TCNQ−TCNQ]$^{2-}$, bidentate *cis*-[μ-TCNQ]$^{-\bullet}$, and two axial MeOH ligands. Distances and angles within (TCNQ−TCNQ)$^{2-}$ (Table 3) are similar to **9**, e.g., the C−C bond joining the dimer is 1.659(10) Å in **10** vs 1.630(13) Å in **9**. The *cis*-[μ-TCNQ]$^{-}$ molecules act as bridging ligands via 1,2-dicyano positions with the two

(12) (a) Lunelli, B.; Pecile, C. *J. Chem. Phys.* **1970**, *52*, 2375. (b) Van Dyne, R. P.; Suchanski, M. R.; Lakovits, J. M.; Siedle, A. R.; Parks, K. D.; Cotton, T. M. *J. Am. Chem. Soc.* **1979**, *101*, 2832. (c) Chappell, J. S.; Bloch, A. N.; Bryden, W. A.; Maxfield, M.; Poehler, T. O.; Cowan, D. O. *J. Am. Chem. Soc.* **1981**, *103*, 2442. (d) Moscherosch, M.; Waldör, E.; Binder, H.; Kaim, W.; Fiedler, J. *Inorg. Chem.* **1995**, *34*, 4326. (e) Inoue, M. B.; Inoue, M.; Fernando, Q.; Nebesny, K. W. *J. Phys. Chem.* **1987**, *91*, 527. (f) Inoue, M.; Inoue, M. B.; *Inorg. Chem.* **1986**, *25*, 37.

(13) Pukacki, W.; Pawlak, M.; Graja, A.; Lequan, M.; Lequan, R. M. *Inorg. Chem.* **1987**, *26*, 1328.

(14) (a) Shields, L. *J. Chem. Soc., Faraday Trans. 2* **1985**, *81*, 1. (b) Humphrey, D. G.; Fallon, G. D.; Murray, K. S. *J. Chem. Soc., Chem. Commun.* **1988,** 1356. (c) Ballester, L.; Barral, M. C.; Gutiérrez, A.; Monge, A.; Perpiñán, M. F.; Ruiz-Valero, C.; Sánchez-Pélaez, A. E. *Inorg. Chem.* **1994**, *33*, 2142. (d) Oshio, H.; Ino, E.; Ito, T.; Maeda. Y. *Bull. Chem. Soc. Jpn.* **1995**, *68*, 889. (e) Kunkeler, P. J.; van Koningsbruggen, P. J.; Cornelissen, J. P.; van der Horst, A. N.; van der Kraan, A. M.; Spek, A. L.; Haasnoot, J. G.; Reedijk, J. *J. Am. Chem. Soc.* **1996**, *118*, 2190. (f) Ballester, L.; Gutiérrez, A.; Perpiñán, M. F.; Amador, U.; Azcondo, M. T.; Sánchez, A. E.; Bellitto, C. *Inorg. Chem.* **1997**, *36*, 6390.

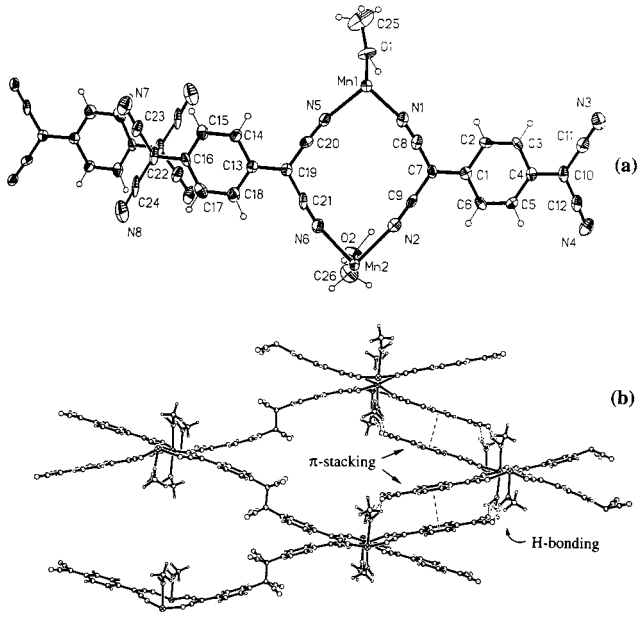

Figure 5. ORTEP diagram of the unique portion of $[Mn(TCNQ)(TCNQ-TCNQ)_{0.5}(MeOH)_2]_\infty$ (**10**) with atoms depicted as 50% probability ellipsoids and (b) side view of the zigzag layers showing interdigitation of two layers stabilized by π-stacking and hydrogen-bonding.

unligated N≡C− groups pointing outward from the edges of the zigzag layers toward axial MeOH ligands in adjacent layers to form hydrogen bonds (N3- - -O2A = 2.834(8) Å and N4- - -O1A = 2.846(8) Å), Figure 5. The metrical parameters within the bidentate $TCNQ^-$ ligand (Table 3) are in accord with data reported for other structures that contain $[TCNQ]^{-\bullet}$.[5,14] In addition to participating in hydrogen bonding, the *cis*-[μ-TCNQ]$^-$ ligands are engaged in π-stacking interactions of 3.295 Å that serve to stabilize a densely packed, interdigitated arrangement of layers (Figure 5b).

$[Mn(TCNQ)_2(H_2O)_2]_\infty$ (11). An ORTEP diagram of the asymmetric unit in **11** is provided in Figure 6a and packing diagrams in the *ab* and *bc* planes are depicted in parts b and c of Figure 6, respectively. The manganese ions are in a pseudo-octahedral environment consisting of four nitrogen atoms from two *syn*-[μ-TCNQ]$^{-\bullet}$ ligands and two axial H_2O molecules. The Mn−N distance of 2.225(2) Å is similar to the corresponding distances observed for the coordinated TCNQ ligands in **9** and **10**, but there are some notable differences (Table 3). The distances within the TCNQ rings in **11** are indicative of the resonance structure in Figure 4c. $[Mn(TCNQ)_2(H_2O)_2]_\infty$ contains alternating single and double bonds in the quinoid ring of the TCNQ, whereas in **9** and **10**, the bonding in the ring is uniform with charge being localized on the exocyclic carbon atom. The extended structure is a 2-D polymeric layered structure with extensive *intra*-layer (~3.1 Å) and *inter*-layer (3.6 Å) π stacking of the $[TCNQ]^{-\bullet}$ radicals. While the latter value is fairly long to be a significant interaction, the 3.1 Å separation between the $[TCNQ]^{-1}$ ligands within the layers is a sign of very strongly coupled π-dimers. Typical ranges for π-$[TCNQ]_2^{2-}$ interactions for selected compounds are provided in Table 4.

$[Zn(TCNQ)(TCNQ-TCNQ)_{0.5}(MeOH)_2]_\infty$ (12). The structure of **12** contains diamagnetic Zn(II) ions and is

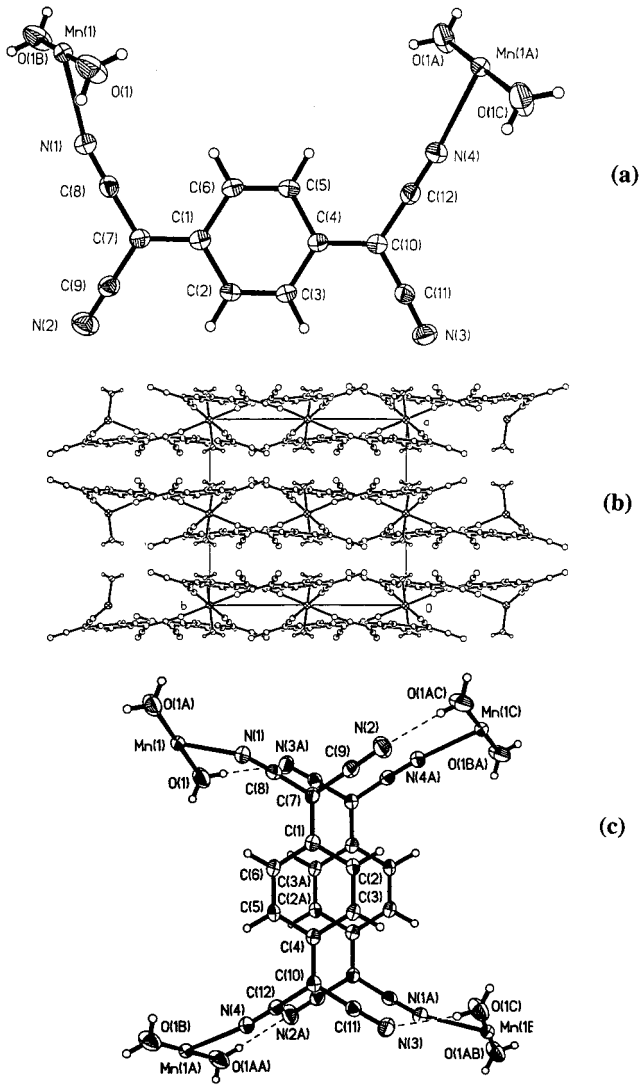

Figure 6. (a) ORTEP diagram of a portion of $[Mn(TCNQ)_2(H_2O)_2]_\infty$ (**11**), (b) side view of the layers viewed in the ab plane and (c) top view of the π-stacking and hydrogen bonding.

essentially identical to that of the Mn analogue (**10**). This is readily apparent from the diagrams in parts a and b of Figure 7. As was found for the Mn analogue, the *cis*-$[TCNQ]^{-\bullet}$ ligands are hydrogen bonded to MeOH molecules via the uncoordinated nitrile positions at distances of (N3- - -O2A = 2.82o(4) Å and N4- - -O1A = 2.865(4) Å). The two different hydrogen bonds distances are N- - -H = 1.72 and 1.77 Å. The intralayer TCNQ−TCNQ π-stacking distance is 3.308 Å.

Infrared Spectroscopic Studies. Infrared spectroscopy in the ν(C≡N) region is useful for assigning charge as well as predicting stacking modes in $TCNQ^{n-}$ salts.[5c,f,12,13] A compilation of these data for **1**−**12** is provided in Table 5. Unfortunately, analysis of IR data for metal-bound TCNQ ligands is complicated by the fact that ν(C≡N) stretches can shift to higher energies if the TCNQ acts primarily as a σ-donor or to lower energies if there is significant metal to TCNQ π-back-bonding.[5f] A more informative infrared active mode is the δ(C−H) bend of TCNQ. We have discovered that this ring-bending mode is a fingerprint for the presence of the σ-dimer $[TCNQ-TCNQ]^{2-}$ vs normal $TCNQ^-$ in the materials.[5c,13] For example, **9** exhibits a δ(C−H) mode at 806 cm^{-1} in accord with the presence of only

Table 4. Stacking Interactions for $TCNQ^-$ Units in Selected Structures

compound	interplanar dist (Å)	binding mode	ref
Rb(TCNQ)	3.16	uncoordinated	15
$(TTP)(TCNQ)_2$	3.22	uncoordinated	15
$[Cu(abpt)_2(TCNQ)_2]$	3.22	monodentate	5c
[Cu(pdto)(TCNQ)]	3.12	bidentate	14b
$NiL^R(TCNQ)_2]$	3.25	monodentate	14c
[Mn(tpa)(TCNQ)(MeOH)](TCNQ)$_2$MeCN	3.05−3.60	monodentate	5d
$[Mn(TCNQ)_2(H_2O)_2]_\infty$	3.1, 3.6[a]	bidentate	this work

[a] Intralayer and interlayer stacking distances, respectively.

Table 5. Infrared Spectroscopic Data in the ν(CN) and δ(C−H) Regions for $TCNQ^-$ Compounds

compound	ν(C≡N), cm^{-1}	δ(C−H), cm^{-1}
TCNQ	2222 (s)	864 (w)
LiTCNQ	2181 (s), 2154 (s)	828 (m)
Compounds with μ-$[TCNQ]^-$ Ligands		
$Mn(TCNQ)_2(H_2O)_2$ (**5**) (bulk)	2211 (s), 2194 (s), 2168 (m)	825 (m)
$Fe(TCNQ)_2(H_2O)_2$ (**6**)	2212 (s), 2195 (s), 2177 (m)	825 (m)
$Co(TCNQ)_2(H_2O)_2$ (**7**)	2220 (s), 2201 (s), 2177 (m)	823 (m)
$Ni(TCNQ)_2(H_2O)_2$ (**8**)	2226 (s), 2208 (s), 2177 (m)	823 (m)
$Mn(TCNQ)_2(H_2O)_2$ (**11**) (crystals)	2206 (s), 2197 (s), 2189 (m), 2166 (sh)	823 (m)
Compounds with μ_4-$[TCNQ-TCNQ]^{2-}$ Ligands		
$[Mn(TCNQ-TCNQ)(MeOH)_4]_\infty$ (**9**)	2202 (s), 2139 (s)	806 (m)
Compounds with μ-$[TCNQ]^{-1}$ and μ_4-$[TCNQ-TCNQ]^{2-}$ Ligands		
$Mn(TCNQ)_2(MeOH)_2$ (**1**)	2214 (s), 2191 (s), 2176 (s), 2159, 2139 (sh)	827 (m), 804 (w)
$Fe(TCNQ)_2(MeOH)_2$ (**2**)	2216 (s), 2187 (s), 2167 (m), 2154 (sh)	827 (m), 802 (w)
$Co(TCNQ)_2(MeOH)_2$ (**3**)	2213 (s), 2189 (s), 2169 (m), 2156 (sh)	825 (m), 804 (w)
$Ni(TCNQ)_2(MeOH)_2$ (**4**)	2224 (s), 2193 (s), 2170 (m), 2158 (sh)	827 (m), 802 (w)
$[Mn(TCNQ)(TCNQ-TCNQ)_{0.5}(MeOH)_2]_\infty$ (**10**)	2216 (s), 2187 (s), 2168 (m), 2156 (sh)	825 (m), 802 (w)
$[Zn(TCNQ)(TCNQ-TCNQ)_{0.5}(MeOH)_2]_\infty$ (**12**)	2222 (s), 2185 (s), 2168 (m)	827 (m), 802 (w)

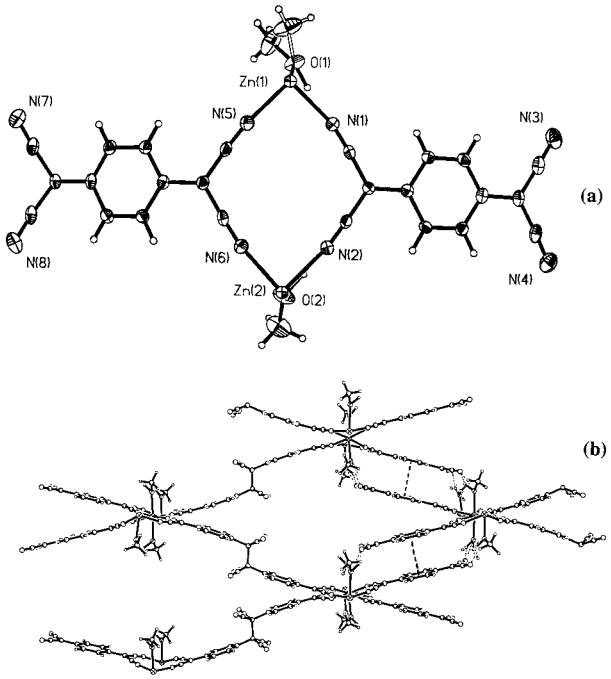

Figure 7. (a) ORTEP diagram and (b) side view of layers in $[Zn(TCNQ)(TCNQ-TCNQ)_{0.5}(MeOH)_2]_\infty$, (**4**).

one type of TCNQ moiety, namely σ−$[TCNQ-TCNQ]^{2-}$. The spectra for **1**, **2**, **3** and **4, 10** and **12**, however, contain features at ∼825 cm^{-1} in addition to one at 802 cm^{-1} which are indications of both $[TCNQ]^{-\bullet}$ and $[TCNQ-TCNQ]^{2-}$ being present. This has been verified in the X-ray structures of **10** and **12**. The spectra of $[Mn(TCNQ)_2(H_2O)_2]_\infty$, (**11**) and the bulk products $Mn(TCNQ)_2(H_2O)_2$ (**5**), $Fe(TCNQ)_2(H_2O)_2$ (**6**), $Ni(TCNQ)_2(H_2O)_2$ (**7**) and $Co(TCNQ)_2(H_2O)_2$ (**8**) exhibit only one δ-(C−H) feature at ∼823 cm^{-1} due to the syn-μ_2-$[TCNQ]^-$ ligand as found in **11**.[14c] The similarities in the IR data between the Mn compounds and the other three metal products prepared in the same solvent strongly support the conclusion that the Fe, Co, and Ni compounds adopt the same structures.

Powder X-ray Diffraction. A room-temperature powder pattern of the bulk sample $Mn(TCNQ)_2(MeOH)_2$ does not appear to resemble the patterns of either **9** and **10** (Figure 8). This is surprising, as IR data indicate that **1** is a physical mixture of **9** and **10**. This incongruity led us to suspect that $Mn(TCNQ)_2(MeOH)_2$ was "decomposing" during the room-temperature powder X-ray experiment to a phase whose structure is similar to the compounds derived from water (Figure 9). To test this hypothesis, X-ray data were obtained at −193 and +25 °C on samples of the bulk material $Mn(TCNQ)_2(MeOH)_2$ (**1**) and on a batch of single crystals of $[Mn(TCNQ-TCNQ)(MeOH)_4]_\infty$ (**9**). In the powder pattern of **1** at −193 °C (Figure 10a), it is possible to discern features due to **9** (Figure 10c) and **10** (not shown).

The differences in the low temperature and room-temperature powder patterns of the MeOH samples have been traced to irreversible cleavage of the fragile C−C bonds in the σ-$[TCNQ-TCNQ]^{2-}$ units under the conditions of X-ray exposure. The basis for this conclusion are the IR data listed in Table 6. As the data clearly show, the δ(C−H) bending mode of $(TCNQ-TCNQ)^{2-}$ at 802 cm^{-1} for compounds **5**−**8, 9**, and **12** disappears or becomes much less prominent after exposure in the X-ray beam at 25 °C; concomitantly, the mode at ∼825 cm^{-1} $(TCNQ)^{1-}$ becomes more intense.

The water-containing samples do not undergo a phase change when exposed to X-rays at room temperature, as evidenced by the results for $Mn(TCNQ)_2(H_2O)_2$ shown in Figure 11. These XRD data point out, however, that the crystals obtained from $MnBr_2$ and LiTCNQ in H_2O (**11**) are not representative of the bulk sample, because

Table 6. Infrared Spectroscopic Data as a Function of Exposure to X-rays

compound	δ(C−H) in cm^{-1} before X-ray exposure	δ(C−H) in cm^{-1} after X-ray exposure
$Mn(TCNQ)_2(MeOH)_2$ (**5**)	827 (m), 804 (w)	825 (m)
$Fe(TCNQ)_2(MeOH)_2$ (**6**)	825 (m), 802 (w)	825 (m)
$Co(TCNQ)_2(MeOH)_2$ (**7**)	825 (m), 804 (w)	823 (m)
$Ni(TCNQ)_2(MeOH)_2$ (**8**)	827 (m), 802 (w)	825 (m), 802 (vw)
$[Mn(TCNQ{-}TCNQ)(MeOH)_4]_\infty$ (**9**)	806 (s)	823 (m), 802 (w)
$[Zn(TCNQ)(TCNQ{-}TCNQ)_{0.5}(MeOH)_2]_\infty$ (**12**)	827 (m), 802 (w)	825 (m)

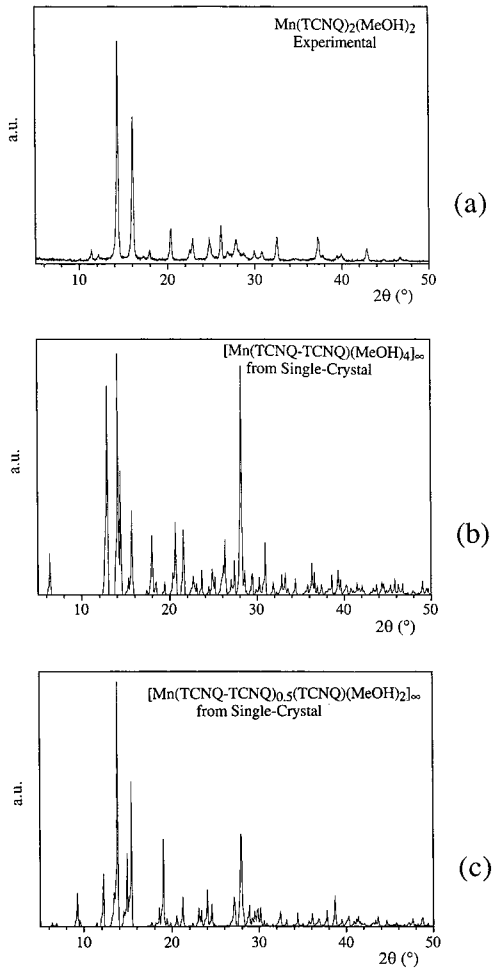

Figure 8. Experimental powder pattern of (a) **1** and simulated powder patterns for (b) **9** and (c) **10**.

the simulated powder pattern for **11** does not match the bulk powder data. Unfortunately, despite numerous screenings of additional crystals grown from H_2O, we have not been able to identify another polymorph of $Mn(TCNQ)_2(H_2O)_2$.

Thermogravimetric Studies. Thermogravimetric analyses of **1**−**8** were performed between 25 and 1000 °C. Representative data for the Mn derivatives are shown in Figure 12. Compounds **1**−**4** lose ∼12% of their mass between 80 and 140 °C, which corresponds to the loss of two methanol molecules. The Mn and Fe samples lose both methanol molecules in one step between 80 and 120 °C whereas the Co and Ni materials gradually lose the methanol over the temperature range of 80−180 °C. Compounds **5**−**8** lose ∼7% of their mass at temperatures below 300 °C which corresponds to two water molecules. Dehydration of $Mn(TCNQ)_2(H_2O)_2$ and $Ni(TCNQ)_2(H_2O)_2$ takes place in essentially one step whereas $Fe(TCNQ)_2(H_2O)_2$ and $Co(TCNQ)_2(H_2O)_2$ lose

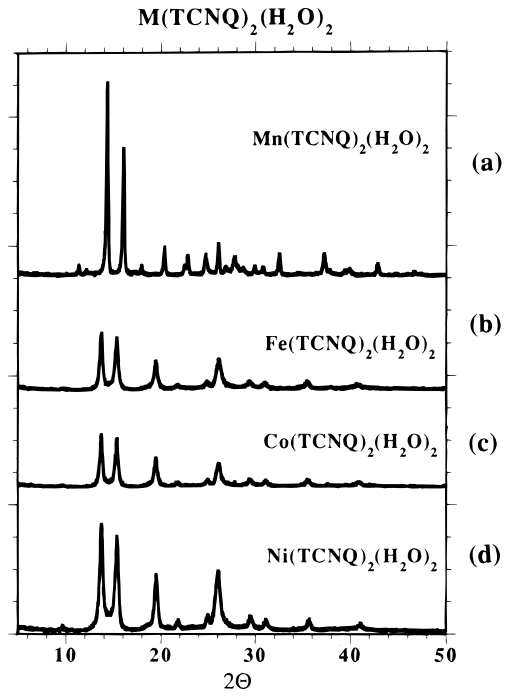

Figure 9. X-ray powder diffraction patterns of bulk samples **5**−**8**.

their water molecules in two steps. After ∼300 °C, all of the compounds experience ∼22% additional mass loss which corresponds to loss of one TCNQ.

Magnetic Properties. Temperature-dependent magnetic susceptibilities (χ) for compounds **1**−**12** were measured from 5 to 300 K in a dc SQUID magnetometer. Plots of χ_{mol}^{corr}, μ_{eff}, and $1/\chi_{mol}^{corr}$ vs temperature for the structurally characterized Mn compounds **9**−**11** are provided in Figures 13−15, whereas the data for compounds **1**−**8**, and **12** are provided as Supporting Information. The results of these studies indicate that the Mn compounds exhibit Curie−Weiss behavior with a small contribution from antiferromagnetic coupling at low temperatures.[15,16] The Ni samples also exhibit Curie−Weiss behavior with small negative Weiss constants whereas the data for the Fe and Co compounds are typical of isolated spin centers of these metals with zero-field splitting effects and orbital contributions. The conclusion that the TCNQ radicals do not contribute to the paramagnetism of these compounds is in accord with the X-ray structures of **9**−**11** that reveal the presence of σ-bonded $[TCNQ{-}TCNQ]^{2-}$ and/or π stacked $[TCNQ]^{-\bullet}$ moieties. Both types of TCNQ- - -TCNQ interactions lead to spin pairing of the organic radicals. In all cases

(15) Dunbar, K. R.; Cowen, J.; Zhao, H.; Heintz, R. A.; Ouyang, X.; Grandinetti, G. *NATO ASI: Supramolecular Engineering of Synthetic Metallic Materials: Conductors and Magnets*; Veciana, J., Ed.; Kluwer: Dordrecht, 1998; The Netherlands, Vol. 518, p 353.

(16) O'Kane, S.; Dunbar, K. R. Unpublished results.

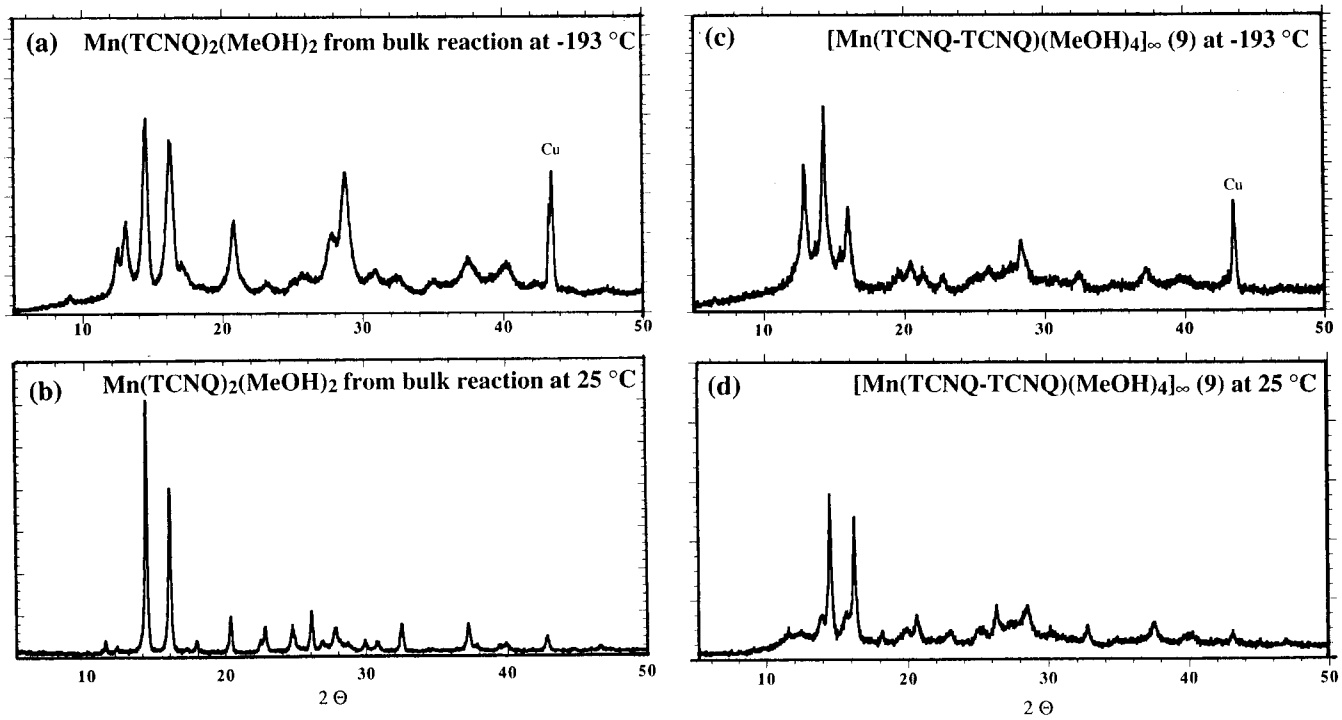

Figure 10. Powder X-ray data at −193 (a, c) and +25 °C (b, d) for bulk (a, b) $Mn(TCNQ)_2(MeOH)_2$ (**1**) and (c, d) $[Mn(TCNQ-TCNQ)(MeOH)_4]_\infty$ (**9**).

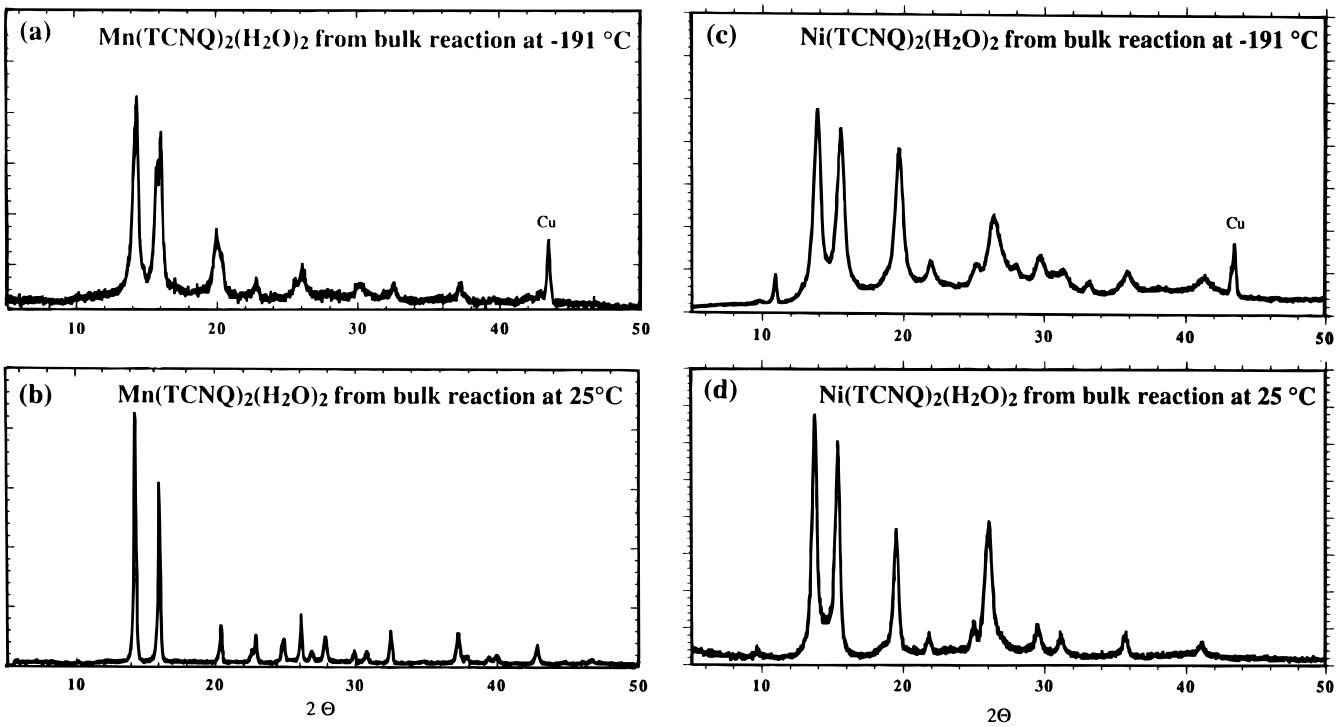

Figure 11. Powder X-ray data at −191 (a, c) and +25 °C (b, d) for bulk (a, b) $[Mn(TCNQ)_2(H_2O)_2]_\infty$ (**5**) and (c, d) $[Ni(TCNQ)_2(H_2O)_2]_\infty$ (**8**).

for the Mn compounds, the values of μ_{eff} are ~5.9 μ_B which is the spin-only value for Mn(II). The fact that the π-stacked $[TCNQ]^{-\bullet}$ ligands in the structure of **10** are diamagnetic was verified by a measurement of the magnetic susceptibility of the isostructural Zn(II) analogue (**12**) which is rigorously diamagnetic.

In considering the role of the σ-dimer $[TCNQ-TCNQ]^{2-}$ in dictating magnetic properties, we heated crystals of $[Mn(TCNQ-TCNQ)(MeOH)_4]_\infty$ (**9**) in the solid-state at 160 °C for 10 h in an effort to break the σ-dimer bond within the $(TCNQ-TCNQ)^{2-}$ ligand. The original sample follows Curie−Weiss behavior, but after heat treatment, the material exhibits a ferromagnetic transition at ~50 K (Figure 16).[15] This new phase can also be formed in situ in an X-ray beam at 220 °C (Figure 17), or by refluxing a suspension of **1** in MeCN for several hours.[16] IR data in the δ(C−H) region indicate that the sample is losing the σ-$(TCNQ-TCNQ)^{2-}$ unit (δ(C−H) = 802 cm^{-1}) and gaining a TCNQ radical unit (δ(C−H) = 823 cm^{-1}). It is interest-

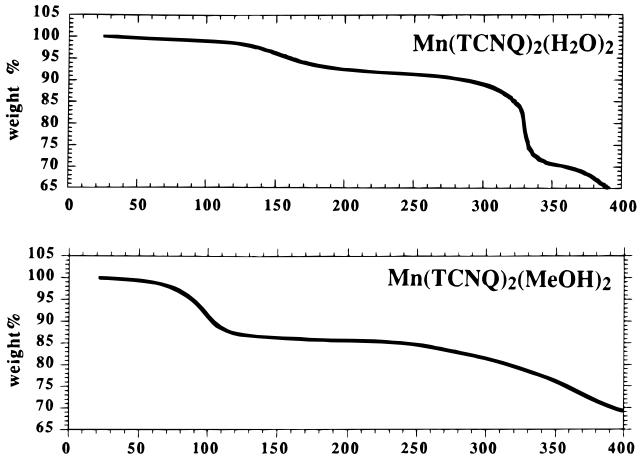

Figure 12. TGA data for the bulk phases $Mn(TCNQ)_2(MeOH)_2$ and $Mn(TCNQ)_2(H_2O)_2$.

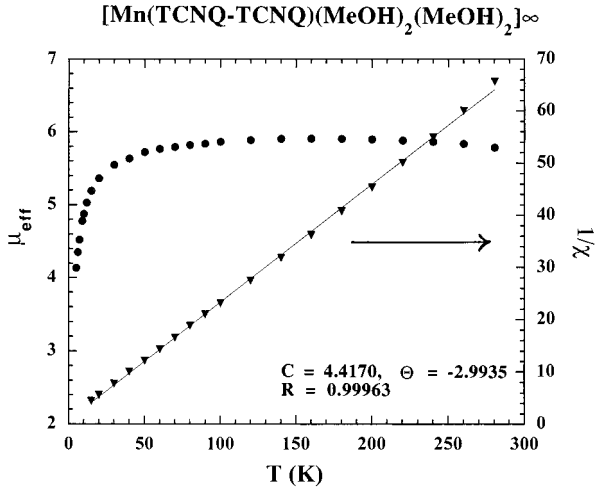

Figure 13. Plots of χ_m, μ_{eff}, and $1/\chi_m$ vs T for (**9**).

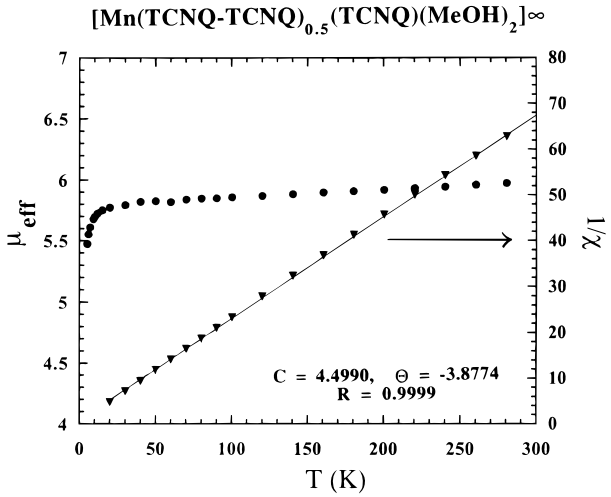

Figure 14. Plots of χ_m, μ_{eff}, and $1/\chi_m$ vs T for (**10**).

ing to note that similar transformations involving the cleavage of the σ-bond in $[TCNE\text{-}TCNE]^{2-}$ dimers have been documented as well.[17]

(17) Zhang, J.; Liable-Sands, L. M.; Rheingold, A. L.; Del Sesto, R. E.; Gordon, D. C.; Burkhart, B. M.; Miller, J. S. *Chem. Commun.* **1998**, 1385.

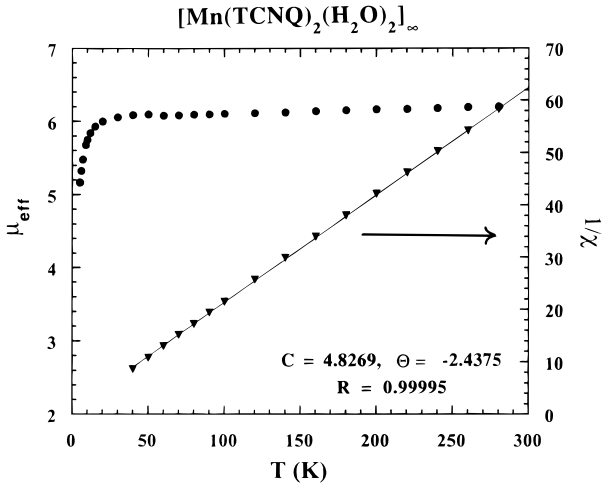

Figure 15. Plots of χ_m, μ_{eff}, and $1/\chi_m$ vs T for (**11**).

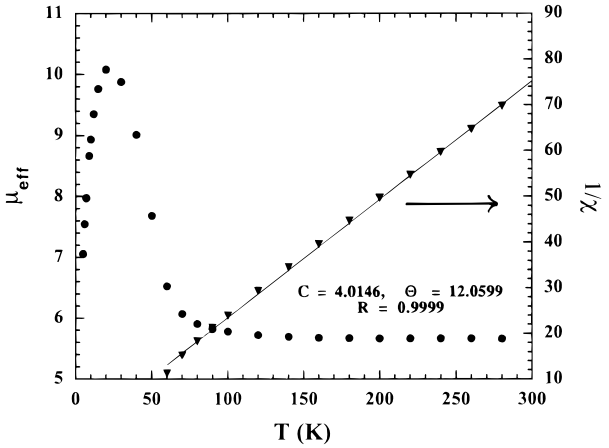

Figure 16. Plots of χ_m, μ_{eff}, and $1/\chi_m$ vs T for (**9**) after heat treatment at 160 °C for 10 h.

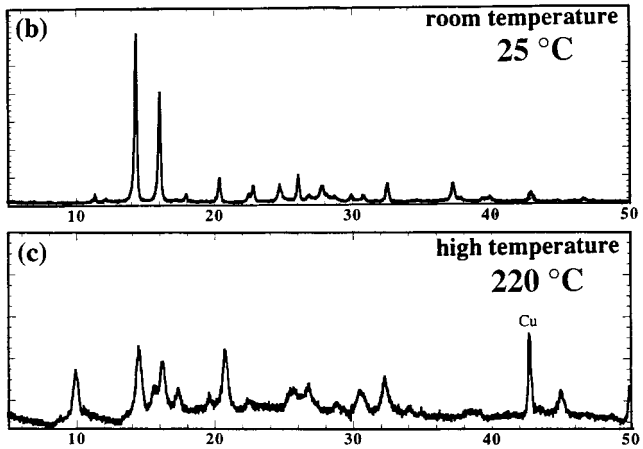

Figure 17. Powder X-ray data for (**9**) at (a) 25 and (b) 220 °C.

Conclusions

These studies reveal that two major products are formed in reactions of Mn(II) ions with $TCNQ^-$ in methanol, *viz.*, $[Mn(TCNQ{-}TCNQ)(MeOH)_4]_\infty$ wherein the metal ions are bridged by μ_4-$[TCNQ{-}TCNQ]^{2-}$ and $[Mn(TCNQ)(TCNQ{-}TCNQ)_{0.5}(MeOH)_2]_\infty$ with both μ_4-$[TCNQ{-}TCNQ]^{2-}$ and *cis*-μ-$[TCNQ]^{-\bullet}$ bridges. The latter structure is also exhibited by the Zn(II) derivative and $[Zn(TCNQ)(TCNQ{-}TCNQ)_{0.5}(MeOH)_2]_\infty$. The X-ray

structure of the layered material $[Mn(TCNQ)_2(H_2O)_2]_\infty$ (**11**) revealed yet another type of $TCNQ^-$ binding, namely *syn*-μ-$[TCNQ]^{-\bullet}$ bridges that participate in strong intralayer π-stacking ($\sim$3.1 Å). These results underscore the importance of solvent and the role of supramolecular interactions (hydrogen-bonding and π-interactions) in stabilizing a particular phase. The diamagnetic σ-$[TCNQ{-}TCNQ]^{2-}$ and π-$[TCNQ]_2^{2-}$ bridges serve to magnetically isolate the $S = {}^5/_2$ Mn(II) centers, as evidenced by the Curie−Weiss behavior of **9**, **10** and **11** between 5 and 300 K ($\mu_{eff} \sim 5.9\ \mu_B$). The methanol materials were found to be unstable with respect to loss of coordinated and interstitial solvent and cleavage of the weak C−C bond in σ-$[TCNQ{-}TCNQ]^{2-}$. The solvent-free crystalline phase that results from heating the paramagnetic material $[Mn(TCNQ{-}TCNQ)(MeOH)_4]_\infty$ in the solid-state is ferromagnetic at low temperatures.

Acknowledgment. K.R.D. gratefully acknowledges the National Science Foundation NSF (CHE-9622589) and The Center for Fundamental Materials Research, Michigan State University for financial support and for funding of the SQUID susceptometers/magnetometers in the Department of Physics & Astronomy at Michigan State University. We also wish to thank Professor T. J. Pinnavaia for the use of his thermogravimetric analysis equipment and Dr. Paul R. Loconto and the NIEHS Basic Superfund Research Center and the Hazardous Substance Research Center at Michigan State University for elemental analyses.

Supporting Information Available: Text giving structure determination information, tables of crystallographic parameters, structure solution and refinement, atomic coordinates, bond distances and angles, anisotropic thermal parameters, and structure factors, and figures showing structures and diffraction data plots for **9**−**12** and figures showing magnetic and thermogravimetric data for compounds **1**−**8** and **12**. This material is available free of charge via the Internet at http://pubs.acs.org.

CM980608V